

Static and dynamic responses of a tied-arch railway bridge under train load

Hongye Gou^{1,2,a}, Biao Yang^{1b}, Wei Guo^{*3,4} and Yi Bao^{5c}

¹Department of Bridge Engineering, School of Civil Engineering, Southwest Jiaotong University, Chengdu 610031, China

²Key Laboratory of High-Speed Railway Engineering, Ministry of Education, Southwest Jiaotong University, Chengdu 610031, China

³School of Civil Engineering, Central South University, Changsha 410075, China

⁴National Engineering Laboratory for High Speed Railway Construction, Changsha 410075, China

⁵Department of Civil, Environmental and Ocean Engineering, Stevens Institute of Technology, NJ 07030 Hoboken, USA

(Received November 5, 2018, Revised March 18, 2019, Accepted March 20, 2019)

Abstract. In this paper, the static and dynamic responses of a tied-arch railway bridge under train load were studied through field tests. The deflection and stresses of the bridge were measured in different static loading scenarios. The dynamic load test of the bridge was carried out under the excitation of running train at different speeds. The dynamic properties of the bridge were investigated in terms of the free vibration characteristics, dynamic coefficients, accelerations, displacements and derailment coefficients. The results indicate that the tie of the measuring point has a significant effect on the vertical movement of the test section. The dynamic responses of arch bridge are insensitive to the number of trains. The derailment coefficients of locomotive and carriage increase with the train speed and symmetrically distributed double-line loads reduce the train derailment probability.

Keywords: tied arch bridge; train load; dynamic response; field test; vertical movement; derailment coefficient

1. Introduction

The rapid economy growth in China drives the development of high-speed railway network (Yan *et al.* 2015). More and more high-speed railway bridges are being constructed. The static and dynamic responses of bridges play an important role in the safe and smooth operation of high-speed trains, and thus have attracted intensive research interests in recent years.

In a railway bridge, the movements of the bridge and trains are coupled due to their direct contact via the wheel and track (Liu *et al.* 2014). Experimental and numerical studies have been conducted on the dynamic performance of bridges under running trains. Finite element models have been established for high-speed train-bridge coupled system under collision to investigate the dynamic characteristics (Xia *et al.* 2014, Li *et al.* 2015, Xia *et al.* 2013, 2018). Therese *et al.* (2018) and Jahangiri *et al.* (2017) respectively established train-track-bridge interaction models to study the dynamic responses of railway bridges and evaluate the operation safety and comfort of the train. Jaber *et al.* (2018) investigated the effects of train speed, track irregularity, and train type on the dynamic behaviors

of six girder bridges for heavy-haul railways. The results showed that the vertical acceleration and dynamic amplification factor (DAF) of simply-supported bridges were significantly influenced by the train speed and track irregularity. Yu *et al.* (2016) and Patrick *et al.* (2015) discussed the effects of track irregularities and train speeds on the random vibration of train-bridge coupling system through experiments and models. Dimitropoulos *et al.* (2015) studied the curve bridges and showed that the centrifugal and coriolis forces induced by the curve controlled the transverse dynamic behaviors of the train-bridge system, when either the curvature or velocity was high. Yang *et al.* (2018) established a three-dimensional finite element model to study the influence of different power spectrums on the buffeting performance of long-span suspension bridges. Mellat *et al.* (2014) carried out field tests and numerical simulations to study the effect of high-speed trains on the dynamic responses of a composite bridge. The maximum vibration magnitude occurred as the train speed reached 320 km/h. Li *et al.* (2016) studied the impact effect, ride and pedestrian comfort, and related parameters for the bridge with moving trains by numerical simulations and experimental tests.

Among the various types of bridges, arch bridges are of special research interest due to the excellent dynamic performance and architectural appearance. Lonetti *et al.* (2016) and Finke (2016) analyzed the dynamic characteristics of tied arch bridges under moving loads through finite element analyses. Cheng *et al.* (2018) conducted finite element simulations of the Yingzhou Bridge, a special-shaped concrete-filled steel tubular arch bridge, and claimed that adding K-shaped struts and reducing the inclination angle of sub-arch effectively improved the transverse stability and stiffness of the bridge.

*Corresponding author, Ph.D., Associate Professor

E-mail: guowei@csu.edu.cn

^a Professor

E-mail: gouhongye@swjtu.cn

^b M.Sc.

E-mail: 2654495832@qq.com

^c Assistant Professor

E-mail: Yi.Bao@stevens.edu

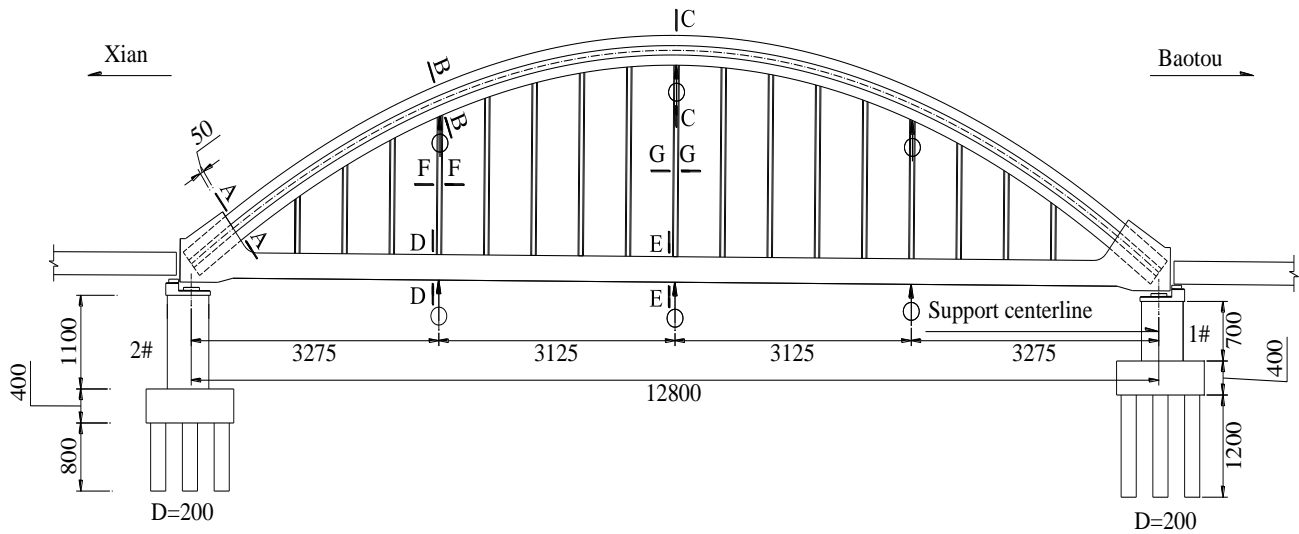


Fig. 1. Elevation view of the bridge and layout of the test section (unit: cm). The circle and arrow in the figure indicate the sections where displacement sensors were deployed

Bayraktar *et al.* (2015) conducted in-situ testing of eight ancient masonry arch bridges and evaluated the vibration frequencies and damping ratios of the bridges. Gou *et al.* (2018a) investigated the dynamic responses of an asymmetrical arch railway bridge under moving trains, and indicated that the dynamic responses of the bridge increased with the train speed and the asymmetrical arrangement of the bridge reduced the structural stiffness. Gou *et al.* (2018b, c) studied the dynamic responses of a straddle-type concrete-filled steel tube tied arch bridge and steel box tied-arch bridge under moving trains. The investigation results showed that the train speed determined the riding comfort of the train. Zhao *et al.* (2016) studied the transverse dynamic mechanical behavior of hangers in a rigid tied-arch bridge under train loads, and concluded that the geometry, cross sectional form, the spatial location of hangers and train speed significantly affected the transverse dynamic mechanical behavior of hangers.

The existing studies show that the model test and field test are the most effective and reliable ways to evaluate the mechanical behaviors of bridges (Gou *et al.* 2018d-h, Pu *et al.* 2018). Computational models are more efficient yet do not always represent the actual situations of train-bridge systems due to the complexity, in particular, for high-speed railway bridges with high requirement of safety and riding comfort (Ticona Melo *et al.* 2018). To date, there still lacks in-situ test data to help understand the dynamic behaviors of train-bridge systems. Meanwhile, there are limited studies on the safety of running trains by measuring the derailment coefficients of the locomotives and carriages.

The primary objective of this study is to study the dynamic responses of a tied-arch high-speed railway bridge. In-situ static and dynamic load tests were conducted, and detailed deflections, accelerations and stresses of the bridge under train loads were measured in real time. The in-situ test data are used to determine the derailment coefficients of locomotives and carriages and evaluate the operation safety of the trains.

2. Description of the bridge

The investigated bridge is a tied-arch railway bridge in the Baotou-Xi'an Railway Line and over the Huangyan Expressway in China. The bridge has a span length of 128 m and a rise height of 25.6 m (Fig. 1). The rise-to-span ratio is 1/5. The longitudinal slope is 7.73‰. The bridge has two parallel arches with a distance of 13.05 m. Each arch has 17 hangers with a 6.25 m spacing; the first hanger is 14 m away from the pivot.

The arch has a concrete-filled steel tube section, as shown in Figs. 2(a) and 2(b). A prestressed concrete girder with a box cross section is used, as shown in Fig. 2(c). The height of the girder is 3.0 m; the width of the girder top is 16.35 m; the width of the girder bottom is 13.69 m. In a 10.5 m length at each end of the girder, the girder top and bottom are widened to 16.95 m and 14.85 m, respectively.

3. Finite element model and In-situ loading tests

3.1 Finite element model

In order to grasp the control section and the arrangement of the train load when the tied-arch bridge is loaded, a finite element model is established to perform the analysis, as shown in Fig.3. In the structural analysis model, the concrete-filled steel tubular ribs are considered as homogeneous materials, and the material properties are obtained by converting the corresponding concrete and steel pipe characteristics (CMR 2012). The main arch rib is simplified as beam element at the arch axis. The transverse brace and the main beam are simulated by beam element, and the boom is simulated by truss element. Rigid connections are used to simulate the connection between the ribs, the transverse braces, the boom and the main beam. Train moving load in finite element analysis is arranged according to "China-live load" (CMR 2017). The main arch rib is divided into 320 elements, the transverse brace is

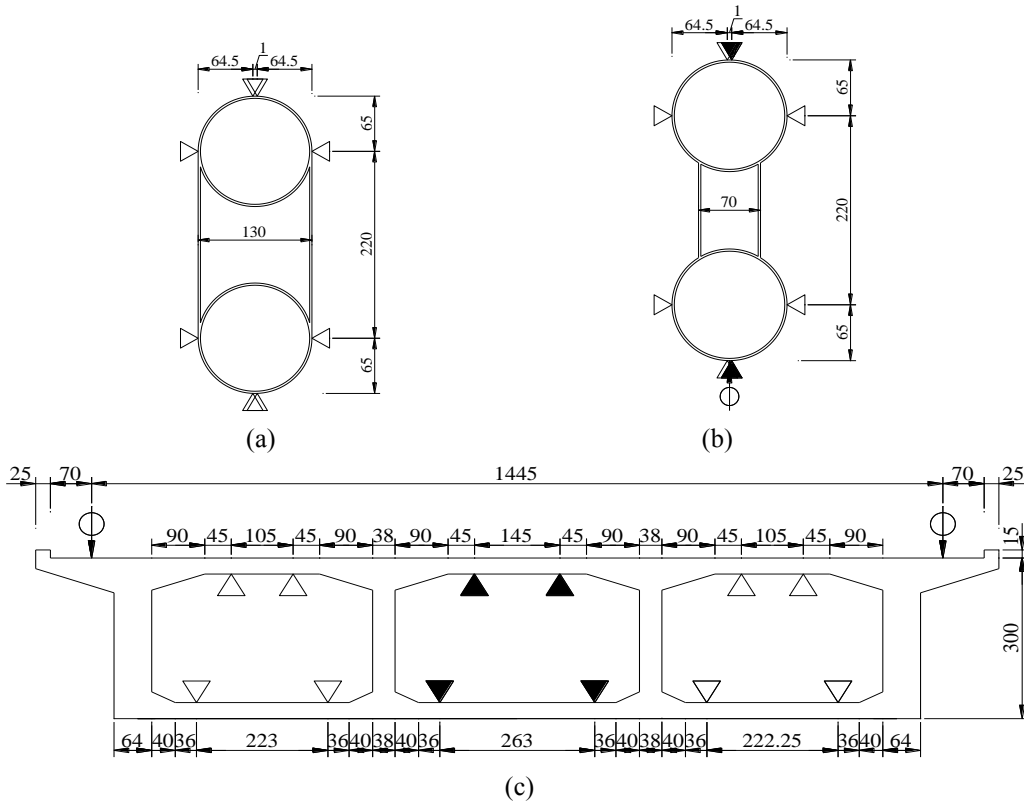


Fig. 2. Schematic diagram of measuring section and measuring point arrangement (unit: cm): (a) section A-A, (b) sections B-B and C-C, (c) sections D-D and E-E. The triangles indicate the locations of strain sensors; the black solid triangles indicate the strain sensors for dynamic measurements. The circle and arrow indicate the locations of displacement sensors.

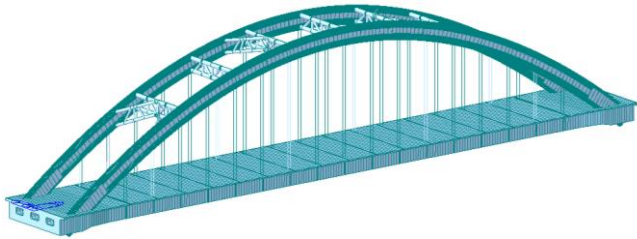


Fig. 3. Finite element model

divided into 265 elements, the boom is divided into 68 elements, and the main beam is divided into 254 elements. The characteristics of the main materials are shown in Table 1. The static deflection, stress and natural vibration characteristics of the bridge structure are also calculated by numerical analysis, and the corresponding results are shown in Tables 2 to 4.

The mass, stiffness and force matrices of the bridge can be obtained by matching principle and the Rayleigh damping is adopted in the finite element model (Gou *et al.* 2018b, i). So the displacement of the bridge system can be expressed by Eq. (1).

$$[\mathbf{M}_b]\{\ddot{\mathbf{Y}}_b\} + [\mathbf{C}_b]\{\dot{\mathbf{Y}}_b\} + [\mathbf{K}_b]\{\mathbf{Y}_b\} = \{\mathbf{F}_{bv}\} \quad (1)$$

Where $[\mathbf{C}_b]$, $[\mathbf{M}_b]$ and $[\mathbf{K}_b]$ are the damping, the mass, and the stiffness matrices of the bridge, respectively; $\{\dot{\mathbf{Y}}_b\}$, $\{\ddot{\mathbf{Y}}_b\}$ and $\{\mathbf{Y}_b\}$ indicate the nodal dynamic acceleration,

Table 1 Material properties

Structure	Material	Elastic modulus	
		(Unit: GPa)	(Unit: MPa)
Girder	C55 concrete	36	
Pier	C35 concrete	33	
The pile cap and the pile foundation	C40 concrete	34	
Steel pipe	Q345 steel	210	
Boom	Steel wire ($\varphi 1 \times 7\text{mm}$)	205	

velocity, and displacement vectors of the bridge; $\{\mathbf{F}_{bv}\}$ indicates the external force vector caused by the moving train.

3.2 Locomotive and carriage

In this study, a locomotive (model: DF8B) and carriages (model: C70) were used to apply the loading. Figs. 4(a) and 4 (b) depict the axle load and wheelbase layout of the locomotive and carriage, respectively. In the locomotive, the wheel diameter is 1050 mm; the axle load is 23 t; the wheelbase layout is 1.8 m + 1.8 m + 8.4 m + 1.8 m + 1.8 m. The maximum speed of the locomotive is 100 km/h. The locomotive has a maximum tractive force of 480 kN. In the carriage, the wheel diameter is 1050 mm; the axle load is 70 t; the wheelbase layout is 1.83 m + 7.38 m + 1.83 m. The maximum speed of the carriage is 100 km/h.

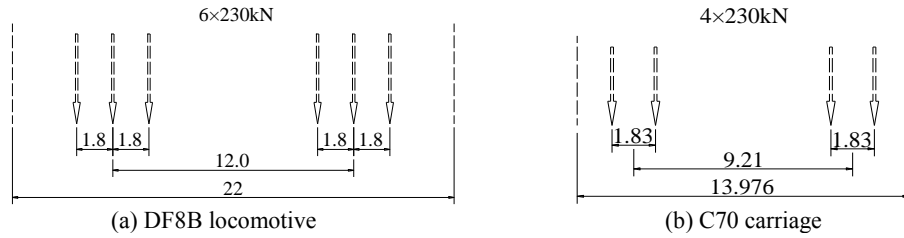


Fig. 4 Schematic diagram of the axle load and wheelbase of locomotive and carriage (unit: m)

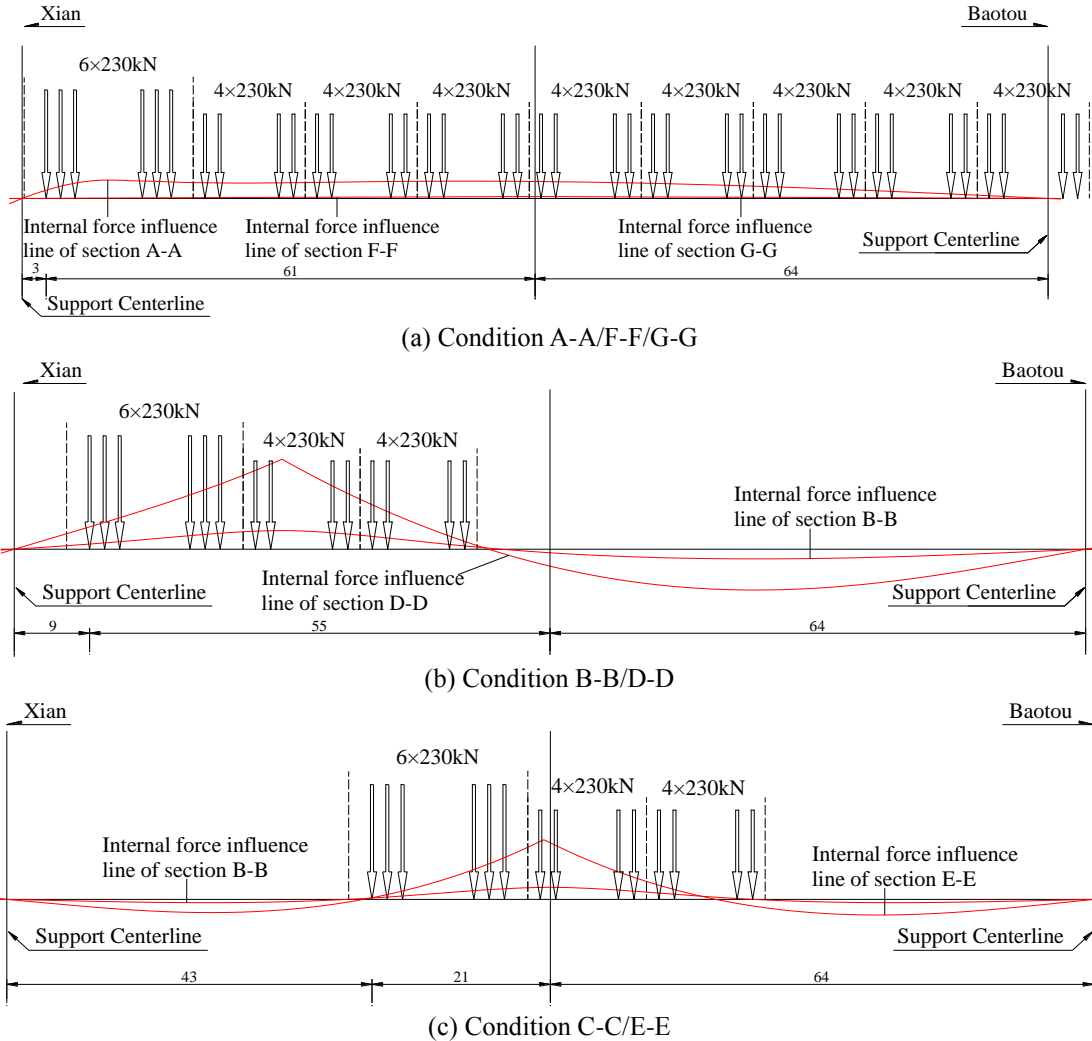


Fig. 5 Layout of locomotive and carriages (unit: m). The red lines are the influence lines of the investigated sections

3.3 Test program

In the static testing, different loading cases were performed to test the different sections of the bridge. The locomotive and carriages were arranged to generate the maximum internal loadings in the investigated sections in the different cases: (1) the maximum moment of the arch foot section A-A, (2) the maximum moment of the hanger section B-B near the quarter span of the arch rib, (3) the maximum moment of the arch vault section C-C, (4) the maximum moment of the quarter span section D-D of the girder, (5) the maximum moment of mid span section E-E of the girder, (6) the maximum axial force of the hanger section F-F near the quarter span of the arch, and (7) the

maximum axial force of the hanger section G-G of the arch. For each case, the most undesired load arrangement was determined through influence line analysis of the bridge, as shown in Fig. 5.

In the dynamic testing, two loading scenarios were investigated: single-line and double-line train loading. For the double-line loading scenario, two trains travelled in opposite directions on the bridge. In either scenario, the train(s) consisted of two locomotives and eight carriages. The two locomotives were at the two ends, and the eight carriages were between the locomotives. The maximum allowable speed of freight train on Bao'xi Railway is 80 km/h. The investigated train speeds include 5, 10, 20, 30, 40, 50, 60, 70 and 80 km/h. The sections B-B, C-C and E-E

were selected for dynamic load test. The pulsation method was used to evaluate the natural frequencies and damping ratios of the bridge.

3.4 Loading locomotives and carriages

Two UCAM-70A and two DEWE-BOOK data acquisition systems were used to collect the static and dynamic load test data, respectively. Ten dial gauges (model: WBD-30) were used to measure the displacements at different sections of the bridge (see Figs. 1 and 2). Two static strain sensors were arranged at the edges of the top and bottom in the sections A-A to C-C, respectively; two static strain sensors were arranged symmetrically on the sides of the top and bottom. A total of 24 static strain sensors were installed on the single side of the arch rib. Six static strain sensors were arranged on the roof and floor in the sections D-D to E-E. A total of 24 static strain sensors were installed in the sections D-D and E-E. Meanwhile, two deflection measuring points were arranged at corresponding positions of the sections B-B to E-E, and the deflection measuring points were symmetrically arranged at the upstream and downstream of the bridge. The whole bridge had a total of 72 static strain sensors and 12 deflection measuring points. As for dynamic load tests, the dynamic strain sensors were only placed at the position of the black triangles in the sections B-B and E-E, as shown in Figs. 2(b) and 2(c). There were 16 dynamic strain measuring points in the whole bridge. In addition, the measuring points of the amplitude and acceleration of the top of pier1# were arranged at the support center line of pier top. The data sampling rate was set to 100 Hz in the data acquisition system.

4. Static test results and discussion

4.1 Deflection

For each variable, the ratio of the measured value to the calculated value is introduced as the checking coefficient, as defined in Eq. (2).

$$\eta = \frac{S_m}{S} \quad (2)$$

where η is the checking coefficient; S_m is the measured value; S is the calculated value.

As shown in Table 2, the error of some positions is large and the checking coefficients are small due to the limitations of the experimental conditions on site and the simplification of the theoretical calculation model. However, the deflection checking coefficients of the bridge are in the range of 0.52 and 0.91, which meets the requirement of the existing China code (CMR 2004), indicating that the bridge has enough stiffness. The checking coefficients of the mid-span are larger than those of the other sections of the girder in all loading cases, suggesting that the elastic performance of the mid-span is better. When the train load is loaded according to the most unfavorable principle, the maximum checking coefficient appears in the test section. Under

Table 2 Checking coefficient of the deflections at different sections

Condition	A-A/F-F/ G-G	B-B /D-D	C-C /E-E
The hanger at the quarter of the arch rib	0.91	0.52	/
Vault	0.89	/	0.88
The hanger at the three quarters of the arch rib	0.6	0.56	0.69
The quarter span of the girder	0.78	0.52	0.78
The mid-span of the girder	0.85	0.7	0.91
The three quarters span of the girder	0.77	0.56	0.75

Table 3 Measured value and calculated value of the stress of sections A-A and B-B (unit: MPa)

Condition and location	Measured value	Calculated value	Relative error (%)	Checking coefficient	
Section (A-A)	The upper edge of the upper chord tube	-7.24	-8.24	12.1	0.88
	The side of the upper chord tube	-6.95	-7.83	11.2	0.89
	The side of the lower chord tube	-2.01	-2.38	15.5	0.84
Section (B-B)	The lower edge of the lower chord tube	-0.93	-1.12	17.0	0.83
	The upper edge of the upper chord tube	-3.86	-4.54	14.9	0.85
	The side of the upper chord tube	-3.72	-4.12	9.7	0.90
	The side of the lower chord tube	-1.29	-1.53	15.7	0.84
	The lower edge of the lower chord tube	/	-1.15	/	/

different loading conditions, the same section has different checking coefficients, which shows that the position of the load has a direct influence on the deflection of the section.

4.2 Stress

Under the condition of static load, the stress test results of the sections A-A and B-B are shown in Table 3. There is a large relative error between the measured value and the calculated value, and the maximum relative error of 17.0%

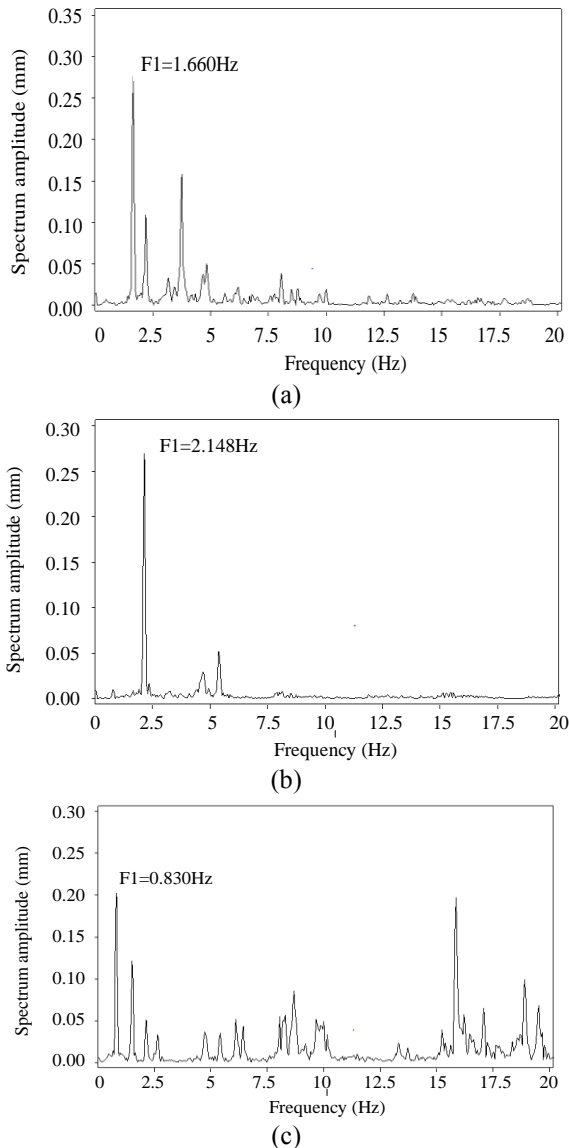


Fig. 6. Dynamic displacement spectra for different bridge components (girder and arch) along different directions: (a) girder along the vertical direction; (b) girder along the transverse direction; (c) arch along the transverse direction.

Table 4 Natural vibration characteristics of the bridge

Vibration mode	Measured (Hz)	Calculated (Hz)	Error (%)	Damping ratio
1st-order transverse bending of the main arch	0.830	0.828	0.24	0.059
1st-order vertical bending of the main girder	1.660	1.642	1.1	0.029
1st-order transverse bending of the main girder	2.148	2.134	0.65	0.023

appears at the arch foot. This can be explained by the fact that the necessary simplification of the finite element

model, and the influence of the temperature, the test load and other conditions (Song 2014). Although the error is large, it is not the standard for evaluating the test and the evaluation index is the checking coefficient specified by the existing China code (CMR 2004). The stress checking coefficients of the bridge structure are in the range of 0.83 and 0.90, which is a reasonable range, indicating that the whole test is reasonable and the bridge structure has enough mechanical strength.

5. Dynamic test results and discussion

5.1 Vibration characteristics

The measurement results of dynamic displacements are used to determine the vibration spectra of the girder and arch through Fast Fourier Transformation (FFT), as shown in Fig. 6.

The transverse fundamental frequency of the arch is 0.830 Hz, which is greater than the value ($f = 90/L = 0.703$ Hz) specified in the China code (CMR 2004), indicating adequate transverse stiffness of the arch. The measured vertical frequency of the girder is 1.66 Hz, which is lower than the measured transverse frequency of 2.148 Hz, indicating that the vertical stiffness of the girder is smaller than its transverse stiffness. The damping ratios of girder along the vertical and transverse directions were determined to be 0.0029 and 0.0023, respectively, through the half-power bandwidth method.

The test and calculation results of the natural vibration characteristics are compared in Table 4. There is only a small error between them, and the measured values are basically consistent with the calculated values. From the analysis of the finite element method in the article written by Rao *et al.* (2017) and Gou *et al.* (2018), it can be known that the errors are caused by multiple reasons. Simplifications are made for the train-bridge system in the calculations; the simulation of support conditions and the stiffness of joints in the finite element model will also influence the vibration frequency of the bridge structure.

5.2 Dynamic coefficients

The ratio of the maximum dynamic response to the maximum static response is defined as the dynamic coefficient. In this paper, strain is used to calculate the dynamic strain coefficient (Pu *et al.* 2011). The formula for calculating the dynamic coefficient is shown in Eq. (3).

$$1 + \mu = \frac{2w_{d\max}}{w_{d\max} + w_{d\min}} = \frac{2\varepsilon_{d\max}}{\varepsilon_{d\max} + \varepsilon_{d\min}} \quad (3)$$

where, $w_{d\max}$ 、 $\varepsilon_{d\max}$ and $w_{d\min}$ 、 $\varepsilon_{d\min}$ are the measured maximum and minimum values of strain, respectively.

Fig. 7 shows the dynamic coefficient curves of each test point under different loading conditions. From the test results, the maximum dynamic coefficients of the quarter of

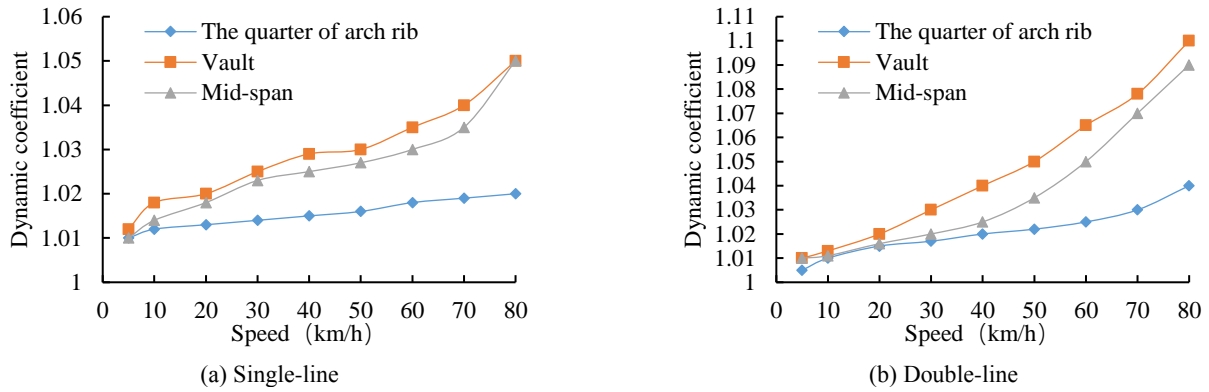


Fig. 7 Dynamic strain coefficients of bridge

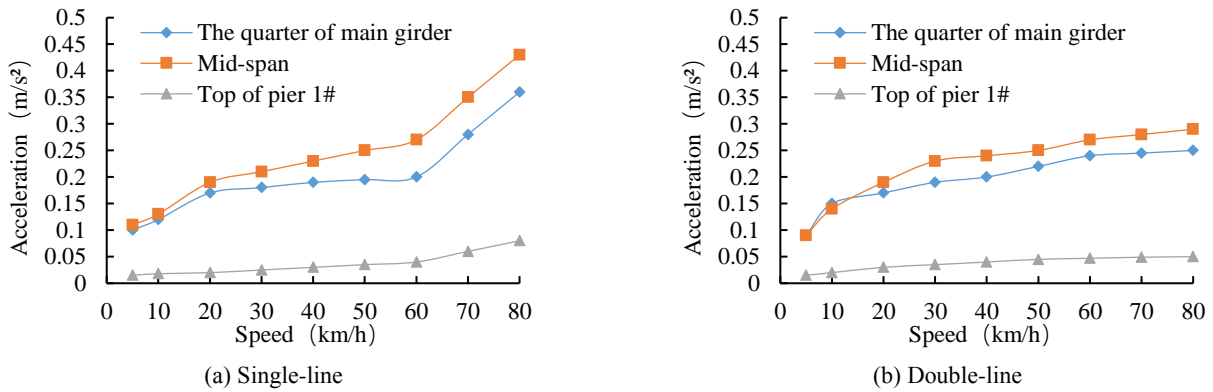


Fig. 8 Measured vertical accelerations of the girder

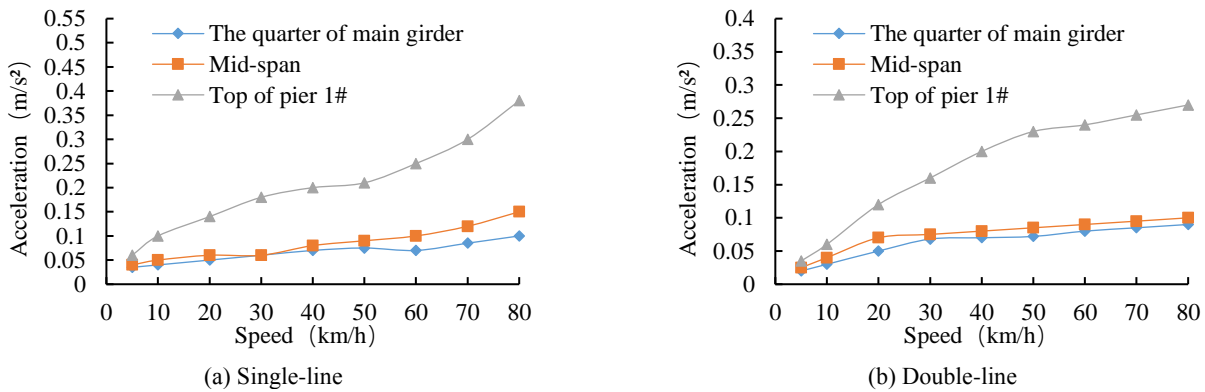


Fig. 9 Measured transverse accelerations of the girder

arch rib, the vault and the mid span of the girder are 1.04, 1.10 and 1.09, respectively. Under the same working conditions, the dynamic coefficients of each test section follow the same trend as the train speed increases. Whether the arch bridge is applied with single line load or double lines load, the dynamic coefficients of each test section increase with the increase of train speed. However, the curve changes faster under the double lines load condition than that under the single line load condition. This is because the dynamic impact of the two trains on the bridge is greater than that of one train

5.3 Accelerations

Figs. 8 and 9 show the peak acceleration curves of each test section along the vertical and transverse directions,

respectively. There is negligible difference between the accelerations in the single-line and double-line loading scenarios. The vertical and transverse accelerations of each test section increase with the train speed. The acceleration of different sections increases slowly with the train speed. As for the mid span and the quarter span of the girder, the vertical acceleration is greater than their transverse acceleration. When the train drives on the bridge at a speed of 80 km/h, the measured maximum transverse acceleration of 0.38 m/s² appears at the top of the pier 1#, which is smaller than the specified value of 1.4 m/s², indicating that the transverse dynamic performance of the bridge structure is good. During the whole test process, the acceleration of each component of the bridge does not increase sharply with the train speed, indicating that the structure did not resonate and the resonance hazard was well avoided.

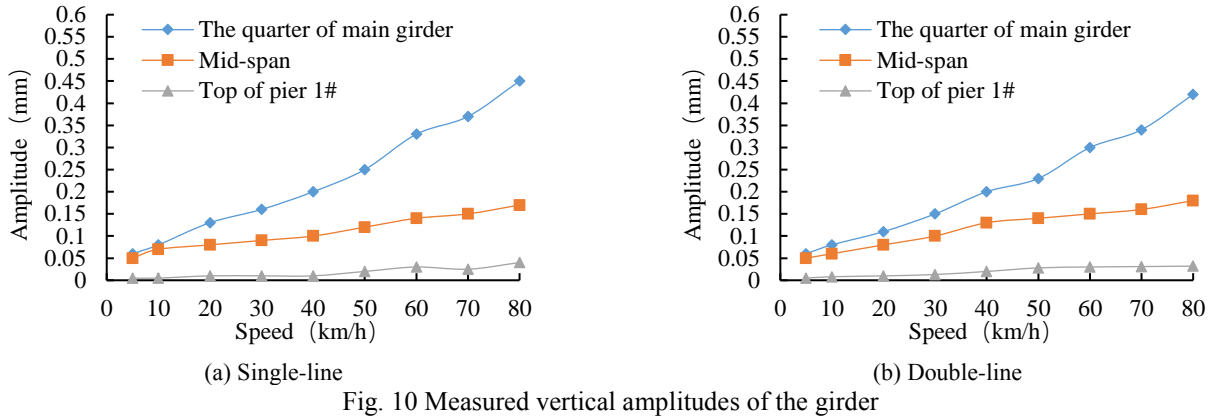


Fig. 10 Measured vertical amplitudes of the girder

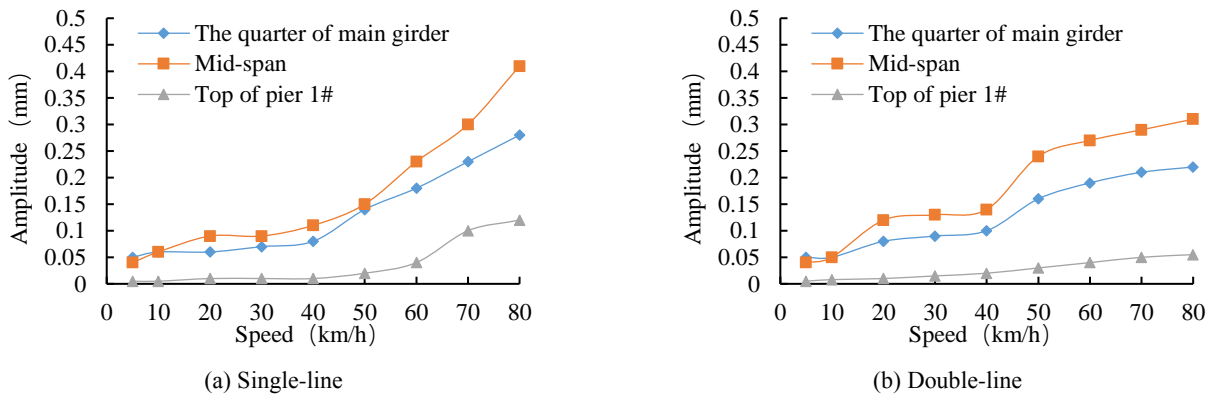


Fig. 11. Measured transverse amplitudes of the girder

5.4 Amplitudes

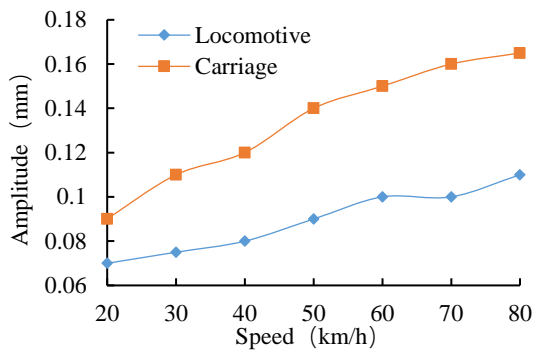
The test results of the amplitude are obtained by analyzing the time history curves of the measured dynamic displacement. Figs. 10 and 11 respectively show the maximum vertical and transverse amplitude of the test sections. There is no obvious difference between the amplitudes in the single-line and double-line loading scenarios. Regardless of the loading scenario, the amplitudes of each test section increase with the train speed. It can be seen from Figs. 10 and 11 that the amplitude of each component of the bridge does not increase sharply with the increase of the train speed, so the structure does not resonate. In the quarter span of the girder, the transverse amplitude is smaller than its vertical amplitude. However, the vertical amplitude is smaller than its transverse amplitude in the mid span of the girder. The reason may be that there are two hangers placed in the mid span section that limits its vertical movement

As for the top of the pier 1#, the difference between the vertical and transverse amplitudes is small. The vertical and transverse stiffness of each test section of the bridge is different, which leads to the different vertical and transverse amplitudes. At the same time, the amplitude of each section under the double-line load is smaller than that under single-line load. This is because the torsion of the girder is reduced under the action of the symmetrical load. When one train drives on single line at a speed of 80 km/h, the maximum vertical amplitude of 0.45 mm occurs at the quarter span of

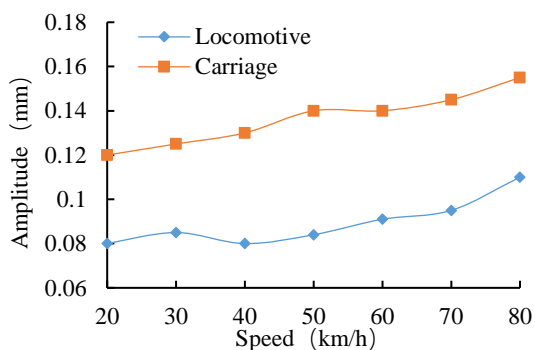
girder, which is about 1/284,444 of the span. Under different loading conditions, the maximum vertical amplitudes of the mid span, the quarter span and the top of pier 1# are 0.18 mm, 0.45 mm and 0.04 mm, respectively, and the maximum transverse amplitudes are 0.41 mm, 0.28 mm and 0.12 mm, respectively. They all meet the requirements of the existing China code (CMR 2004).

5.5 Derailment coefficients

Fig. 12 shows the derailment coefficients of the locomotive and carriage. As the train speed increases, the derailment coefficients increase. Based on the value of the derailment coefficient of the running train, it is usually possible to analyze the derailment probability (Wang *et al.* 2018, Ling *et al.* 2014). Under the single-line and double-line load conditions, the derailment coefficients of the locomotive and carriage increase with the train speed. The maximum derailment coefficients of the locomotive and carriage are 0.11 and 0.17, respectively, not exceeding the limit value (0.8) as specified in the design provisions (CMR 2014). Regardless of the type of load excitation, the safety of the locomotive and carriage meets the requirements of the code when the train passes over the bridge. Another observation is that the derailment coefficients of locomotive are smaller than that of the carriage at the same train speed. Therefore, the running safety of the locomotive and carriage should be studied separately.



(a) Single-line



(b) Double-line

Fig. 12 Derailment coefficient of the locomotive and carriage

6. Conclusions

Based on the above load test studies, the conclusions can be summarized as follows:

- The elastic working performance of the mid span of girder is better than that of other test sections of girder. The same section has different checking coefficients under different loading conditions, which shows that the loading position influences the responses. The bridge has enough stiffness and strength in compliance with the design requirements.
- The transverse stiffness of the arch of the bridge is adequate. As for the girder, the transverse natural frequency is larger than the vertical natural frequency, indicating that the transverse stiffness of bridge structure is greater than the vertical stiffness.
- The dynamic impact on the bridge is small when the train is driving on the bridge. When two trains drive at 80 km/h, the measured dynamic coefficient reaches the maximum (1.10) at the vault.
- The acceleration response of the test sections is insensitive to the number of loaded trains. But the vertical and transverse accelerations are both increasing with the increase of train speed.
- The vertical amplitude of the mid-span section is less than that of the quarter span section in all loading conditions, because the mid-span section has two hangers

that limit the vertical movement of the girder. When one train runs on the single line at 80 km/h, the maximum vertical amplitude of 0.45 mm is measured at the quarter span of the girder.

- The derailment coefficients of locomotive and carriage increase with the train speed. The derailment coefficient of the locomotive and carriage under double-line load is less than that under single-line load. The derailment coefficient of the carriage plays a decisive role for the riding safety of the train.

Acknowledgments

The research was funded by the National Natural Science Foundation of China (Grant No. 51878563), the Sichuan Science and Technology Program (Grant No. 2018JY0294 and 2018JY0549), and the Ministry of Science and Technology of China (Grant No. KY201801005).

References

- Bayraktar, A., Türker, T. and Altunişik, A.C. (2015), "Experimental frequencies and damping ratios for historical masonry arch bridges", *Constr. Build. Mater.*, **75**, 234-241. <https://doi.org/10.1016/j.conbuildmat.2014.10.044>.
- Cheng, X.X., Dong, J., Cao, S.S., Han, X.L. and Miao, C.Q. (2018), "Static and dynamic structural performances of a special-shaped concrete-filled steel tubular arch bridge in extreme events using a validated computational model", *Arab. J. Sci. Eng.*, **43**(4), 1839-1863. <https://doi.org/10.1007/s13369-017-2771-0>.
- CMR (2012), Technical specification for concrete-filled steel tubular structures, (In Chinese).
- CMR (2014), Code for design on railway bridge and culvert, (In Chinese).
- CMR 120 (2004), Code for rating existing railway bridge, (In Chinese).
- CMR 285 (2005). Interim design provisions for the new railway shared lines of passenger and freight trains at 200 km/h. (In Chinese)
- Dimitrakopoulos, E.G. and Zeng, Q. (2015), "A three-dimensional dynamic analysis scheme for the interaction between trains and curved railway bridges", *Comput. Struct.*, **149**, 43-60. <https://doi.org/10.1016/j.compstruc.2014.12.002>.
- Finke, J.E. (2016), "Static and dynamic characterization of tied arch bridges", Ph.D. Dissertation, Missouri University of Science and Technology, USA.
- Gou, H.Y., He, Y.N., Zhou, W., Bao, Y. and Chen, G.D. (2018a), "Experimental and numerical investigations of the dynamic responses of an asymmetrical arch railway bridge", *P. I. Mech. Eng. F-J. Rai.*, **232**(9), 2309-2323. <https://doi.org/10.1177/0954409718766929>.
- Gou, H.Y., Zhou, W., Yang C.W., Bao, Y. and Pu, Q.H. (2018b), "Dynamic response of long-span concrete-filled steel tube tied arch bridge and riding comfort of monorail trains", *Appl. Sci.*, **8**(4), 2076-3417. <https://doi.org/10.3390/app8040650>.
- Gou, H.Y., Zhou, W., Chen, G.D., Bao, Y. and Pu, Q.H. (2018c), "In-situ test and dynamic analysis of a double-deck tied-arch bridge", *Steel Compos. Struct.*, **27** (2), 161-175.
- Gou, H.Y., Zhou, W., Bao, Y., Li, X.B. and Pu, Q.H. (2018d), "Experimental study on dynamic effects of a long-span railway continuous beam bridge", *Appl. Sci.*, **8**(5), 2076-3417.
- Gou, H.Y., Long, H., Bao, Y., Chen, G.D., Pu, Q.H. and Kang, R.

- (2018e), “Experimental and numerical studies on stress distributions in girder-arch-pier connections of long-span continuous rigid frame arch railway bridge”, *J. Bridge Eng.*, **23**(7), 04018039.
- Gou, H.Y., Wang, W., Shi, X.Y., Pu, Q.H. and Kang, R. (2018f), “Behavior of steel-concrete composite cable anchorage system”, *Steel Compos. Struct.*, **26**(1), 115-123. <https://doi.org/10.12989/scs.2018.26.1.115>.
- Gou, H.Y., Shi, X.Y., Zhou, W., Cui, K. and Pu, Q.H. (2018g), “Dynamic performance of continuous railway bridges: Numerical analyses and field tests”, *P. I. Mech. Eng. F-J. Rai.*, **232**(3), 936-955. <https://doi.org/10.1177/0954409717702019>.
- Gou, H.Y., Yang, L.C., Leng, D., Bao, Y. and Pu, Q.H. (2018h), “Effect of bridge lateral deformation on track geometry of high-speed railway”, *Steel Compos. Struct.*, **29**(2): 219-229. <https://doi.org/10.12989/scs.2018.29.2.219>.
- Gou, H.Y., Long, H., Bao, Y., Chen, G.D. and Pu, Q.H. (2018i), “Dynamic behavior of hybrid framed arch railway bridge under moving trains”, *Steel Compos. Struct.*, <https://doi.org/10.1080/15732479.2019.1594314>.
- Jahangiri, M. and Zakeri, J. A. (2017), “Dynamic analysis of train-bridge system under one-way and two-way high-speed train passing”, *Struct. Eng. Mech.*, **64**(1), 33-44. <https://doi.org/10.1080/15732479.2019.1594314>.
- Jaber, M., Zakeri, J. A. and Mohamadzadeh, S. (2018), “Field and numerical investigation of the effect of under-sleeper pads on the dynamic behavior of railway bridges”, *P. I. Mech. Eng. F-J. Rai.*, <https://doi.org/10.1177/0954409718764027>.
- Liu, K., Zhang, N., Xia, H. and Roeck, G. D. (2014), “A comparison of different solution algorithms for the numerical analysis of vehicle-bridge interaction”, *Int. J. Struct. Stab. Dy.*, **14**(02), 1350065. <https://doi.org/10.1142/S021945541350065X>.
- Li, X., Liu, Q., Pei, S., Song, L. and Zhang, X. (2015), “Structure-borne noise of railway composite bridge: Numerical simulation and experimental validation”, *J. Sound Vib.*, **353**, 378-394. <https://doi.org/10.1016/j.jsv.2015.05.030>.
- Li, Y., Cai, C. S., Liu, Y., Chen, Y. and Liu, J. (2016), “Dynamic analysis of a large span specially shaped hybrid girder bridge with concrete-filled steel tube arches”, *Eng. Struct.*, **106**, 243-260. <https://doi.org/10.1016/j.engstruct.2015.10.026>.
- Lonetti, P., Pascuzzo, A. and Davanzo, A. (2016), “Dynamic behavior of tied-arch bridges under the action of moving loads”, *Math. Probl. Eng.*, <http://dx.doi.org/10.1155/2016/2749720>.
- Ling, L., Xiao, X. B. and Jin, X. S. (2014), “Development of a simulation model for dynamic derailment analysis of high-speed trains”, *Acta Mech. Sinica*, **30**(6), 860-875. <https://doi.org/10.1007/s10409-014-0111-0>.
- Mellat, P., Andersson, A., Pettersson, L. and Karoumi, R. (2014), “Dynamic behaviour of a short span soil-steel composite bridge for high-speed railways-Field measurements and FE-analysis”, *Eng. Struct.*, **69**, 49-61. <https://doi.org/10.1016/j.engstruct.2014.03.004>.
- Patrick, S. and Adam, C. (2015), “Modeling of dynamic train-bridge interaction in high-speed railways”, *Acta Mech.*, **226**(8), 2473-2495. <https://doi.org/10.1007/s00707-015-1314-6>.
- Pu, Q.H., Wei, Z.L. and Li, X.B. (2011), “Study on dynamic coefficient influence factors of continuous steel truss arch bridge with large span”, *J. Earthq. Eng. Eng. Vib.*, **31**(6), 0123-0128.
- Pu, Q.H., Wang, H.Y., Gou, H.Y., Bao, Y. and Yan, M. (2018), “Fatigue Behavior of Prestressed Concrete Beam for Straddle-Type Monorail Tracks”, *Appl. Sci.*, **8**(7), 1136. <https://doi.org/10.3390/app8071136>.
- Rao, S.S. (2017), *The Finite Element Method in Engineering*, Butterworth-Heinemann, United Kingdom.
- Song, L.L. (2014), “Bridge load testing structural verification ratio influence analysis”, M.Sc. Dissertation, Chang An University, China.
- Therese, A. (2018), “Train-track-bridge interaction for the analysis of railway bridges and train running safety”, Ph.D. Dissertation, KTH Royal Institute of Technology, Sweden.
- Ticona Melo, L. R., Bittencourt, T. N., Ribeiro, D. and Calçada, R. (2018), “Dynamic response of a railway bridge to heavy axle-load trains considering vehicle-bridge interaction”, *Int. J. Struct. Stab. Dy.*, **18**(01), <https://doi.org/10.1142/S0219455418500104>.
- Wang, J. T., Hai, J., Li, X. Y. and Zhang, Y. (2018), “A study of the mechanism of the effect of the lateral deviation of the barycenter of cargoes on the safety of an open-topped train running a curved railroad”, *Traffic Engineering and Technology for National Defence*, 10-14.
- Xia, C. Y., Xia, H. and Roeck, G. De (2014), “Dynamic response of a train-bridge system under collision loads and running safety evaluation of high-speed trains”, *Comput. Struct.*, **140**, 23-38. <https://doi.org/10.1016/j.compstruc.2014.04.010>.
- Xia, C., Xia, H., Zhang, N. and Guo, W. (2013), “Effect of truck collision on dynamic response of train-bridge systems and running safety of High-speed trains”, *Int. J. Struct. Stab. Dy.*, **13**(03), 1250064. <https://doi.org/10.1142/S0219455412500642>.
- Xia, C., Ma, Q., Song, F., Wu, X. and Xia, H. (2018), “Dynamic analysis of high-speed railway train-bridge system after barge collision”, *Struct. Eng. Mech.*, **67**(1), 9-20. <https://doi.org/10.12989/sem.2018.67.1.009>.
- Yan, B., Gong, L. D. and Nan, H. (2015), “Recent development of design and construction of short span high-speed railway bridges in China”, *Eng. Struct.*, **100**, 707-717. <https://doi.org/10.1016/j.engstruct.2015.06.050>.
- Yu, Z. W., Mao, J. F., Guo, F. Q. and Guo, W. (2016), “Non-stationary random vibration analysis of a 3D train-bridge system using the probability density evolution method”, *J. Sound Vib.*, **366**, 173-189. <https://doi.org/10.1016/j.jsv.2015.12.002>.
- Yang, Y., Gang, Y., Wei, F. and Qin, W. (2018), “Buffeting performance of long-span suspension bridge based on measured wind data in a mountainous region”, *J. Vibroeng.*, **20**(1). <https://doi.org/10.21595/jve.2017.18737>.
- Zhao, H.W., Ding, Y.L., An, Y.H. and Li, A.Q. (2016), “Transverse dynamic mechanical behavior of hangers in the rigid tied-arch bridge under train loads”, *J. Perform. Constr. Fac.*, **31**(1), 04016072. [https://doi.org/10.1061/\(ASCE\)CF.1943-5509.0000932](https://doi.org/10.1061/(ASCE)CF.1943-5509.0000932).

PL